New Two-Stage Accelerator for Hypervelocity Impact Simulation

E.B. Igenbergs*
Technische Universität Munchen, Federal Republic of Germany
and
D.W. Jex† and E.L. Shriver†
NASA Marshall Space Flight Center, Huntsville, Ala.

The present knowledge of the micrometeoriod environment and the simulation requirements for laboratory devices show that the simulated mass-velocity range must be extended to higher values in both mass and velocity. This is accomplished with the new two-stage accelerator, which consists of a light gas gun as the first stage and a coaxial accelerator with a compressor coil as the second stage. The operation of the new device is described together with a theoretical investigation of the timing of the first and the second stage, which leads to an appropriate adjustment of the two stages. The theoretical and experimental results agree well and show that 600-μ diameter glass beads have been accelerated to velocities near 20 km/sec.

Nomenclature

a	= ratio of outer and inner electrodes in coaxial accelerator
A	= magnetic field function, 1/m, area, m^2
b	= gradient of inductivity, henry/m
B	= magnetic induction = H, gauss
c	= drag coefficient
C	= capicitance, farads
E	= electric field, v/m
F	= force, Newtons
H	= magnetic field, A/m
I	= electric current, amp
j	= electric current density, amp/m^2
L	= inductivity, henry
m	= mass, kg
p	= pressure, N/m^2
r	= radius, radial coordinate, meters
R	= ohmic resistance, gas constant, ohm, radius
t	= time, time coordinate, sec
T	= temperature, K
U	= voltage
v	= velocity, km/sec
z	= axial coordinate, meters
σ	= electrical conductivity, 1/ohm m
ϕ	= azimuthal coordinate
μ	= magnetic susceptibility
q	= density, kg/m^3
χ	= polytropical exponent
∇	= nabla operator
Δ	= finite difference

Subscripts

0	= time = 0
1	= right-hand equivalent circuit mesh
2	= left-hand equivalent circuit mesh
z	= axial
r	= radial
ϕ	= azimuthal
c	= compressor coil
d	= delay
D	= drag
e	= center electrode
p	= projectile

Received August 26, 1974; revision received January 14, 1975. The authors wish to thank E. Stuhlinger, G. Bucher, and R. Naumann of the NASA Marshall Space Flight Center, Huntsville, Alabama and H.O. Ruppe and H. Kuczera of the Technische Universität Munchen for the support of the experimental and theoretical investigations. The computations were performed at the Leibniz Rechenzentrum, Bayerische Akademie der Wissenschaften, Munich.

Index categories: Hypervelocity Impact; Plasma Dynamics and MHD.

*Oberingenieur, Institut fur Raumfahrttechnik.
†Research Scientists, Space Sciences Laboratory.

I. Introduction

THE present knowledge of the environment in cislunar, translunar and interplanetary space[1,2] defines the simulation requirements for laboratory devices in which small particles with a density between 0.5 and 4.0 g/cm^3, and a mass between 10^{-15} and 1 grams are accelerated to the velocity of micrometeoriods. The velocity distribution of the micrometeoriods in space indicates 20 km/sec as the most probable velocity.[2] With the mass distribution from Ref. 2 and more recent observations,[3] the mass/velocity in which micrometeoriod impact would most probably occur is defined as shown in Fig. 1. This figure also shows the mass/velocity range simulated by laboratory devices.

A survey of the accelerators used for micrometeoriod simulation is found in Refs. 4, 5, and 7. All of these accelerators simulate a portion of the mass/velocity range of interest, as shown in Fig. 1.

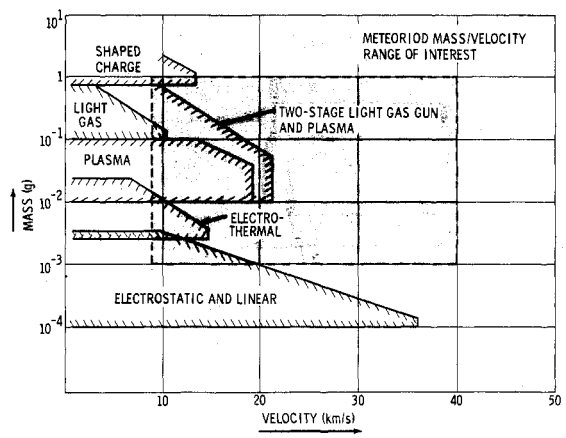

Fig. 1 Mass-velocity diagram of micrometeoriod environment with areas simulated by the different devices.

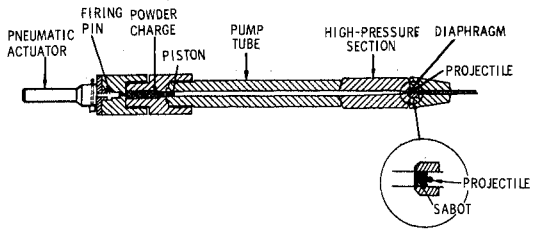

Fig. 2 Light gas gun used in the experiments as first stage.

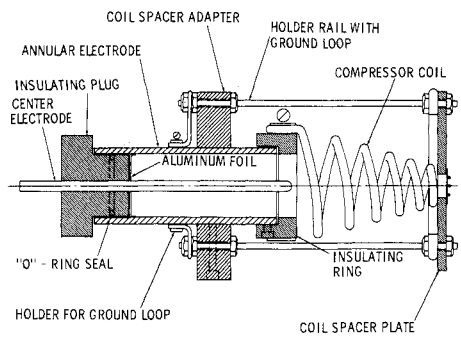

Fig. 3 Coaxial plasma accelerator with compressor coil used in the experiments as second stage.

The most frequently used device is the light gas gun, which is part of the highly developed ballistic range technology, see Fig. 2. This device is used as the first stage in the two-stage accelerator described in Sec. II.

An improvement of the coaxial accelerator has been achieved (shown in Fig. 3) using a compressor coil.[8] A version of this device is used as the second stage in the new two-stage accelerator. Figure 1 shows that the coaxial accelerator with compressor coil (labeled plasma) and the two-stage accelerator contribute significantly to the simulation capability.

II. Description and Operation

The two-stage accelerator consists of a light gas gun as the first stage and a coaxial plasma accelerator with compressor coil as the second stage. The light gas gun is shown in Fig. 2. It has a powder charge for initiating the acceleration process, a piston for compressing the light gas used as the projectile driver, and a pump tube to supply the initial reservoir for the light gas used. The light gas reservoir is separated from the barrel and the projectile by a diaphragm.

To begin the acceleration process, a pneumatic actuator ignites the powder charge. The powder charge gas expansion accelerates the piston and compresses the gas in the reservoir. The diaphragm will rupture at a known pressure of the compressed light gas. The sabot and the projectile are accelerated in the barrel by the expansion of the compressed light gas. For maximum performance, the pump tube should be filled with hydrogen; but in these experiments helium was used for safety reasons. Glass beads with a diameter of 600 μ were accelerated to an average velocity of 3.8 km/sec by the light gas accelerator.

The second stage is a coaxial accelerator with compressor coil; an example is shown in Fig. 3. The positive side of a charged capacitor bank (270 μf, 20 kv maximum charging voltage) is connected via a discharge switch to the center electrode, which is separated by an insulating plug from the annular electrode. Prior to the discharge, an aluminum foil is installed connecting the center and annular electrode. The annular electrode is connected to the negative side of the capacitor bank. An insulating ring separates the compressor coil from the annular electrode. The holder rail with ground loop connects the front end of the compressor coil to the annular electrode. At the beginning of the discharge the annular electrode is at a negative potential. The front end of the compressor coil is held in place by the coil spacer plate.

After the discharge switch is activated, the current evaporates the aluminum foil and generates an aluminum plasma. The discharge current density from center electrode to annular electrode will interact with the azimuthal magnetic field around the center electrode and will accelerate the plasma axially. After the plasma has entered the compressor coil, there will also be a discharge between the center electrode tip and the compressor coil. The current in the compressor coil windings generates a magnetic field which interacts with the plasma flow. This results in a compression and an axial acceleration of the plasma. A fast, high-density flow is generated that can accelerate the projectiles which are exposed to the flow by gasdynamic drag. In the experiments conducted so far with this device, glass beads with a diameter of 250 μ were accelerated to velocities near 20 km/sec.[9,10] The new two-stage accelerator is shown in Fig. 4. The light gas gun barrel is used as a center electrode of the coaxial plasma accelerator. The glass beads are accelerated in the light gas gun first stage and then enter the compressor coil of the plasma accelerator along the axis of symmetry. There the beads can be accelerated by the fast, high-density plasma flow of the second stage.

The two-stage operation begins with the loading of the light gas gun with beads and powder and with the insertion of the aluminum foil into the second stage coaxial plasma accelerator. Then the capacitor bank is charged to the preselected value. The acceleration is initiated by the ignition of the light gas gun powder charge. The shock wave in front of the beads traveling along the light gas gun barrel generates a light flash at the muzzle. This signal is detected by a transient light detector which triggers a delay generator. After a preset delay, this generator triggers the thyratron firing circuit, which, in

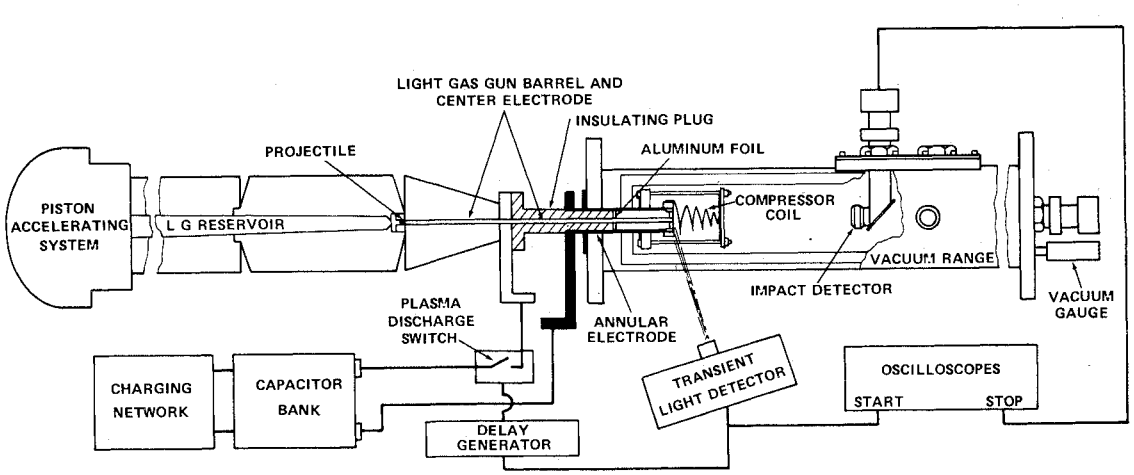

Fig. 4 Two-stage accelerator with timing setup.

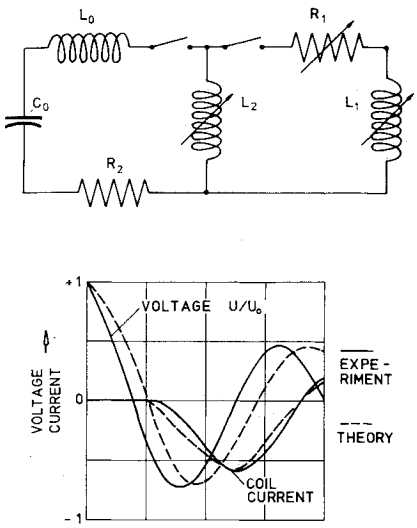

Fig. 5 Equivalent circuit and theoretical and experimental curves for compressor coil current and capacitor bank voltage.

turn, gives a firing pulse to the ignitrons of the capacitor bank. There is a time interval of 2 μsec between the output of the delay generator and the beginning of the capacitor bank discharge.

The successful operation of the two-stage accelerator depends upon the proper timing of the two stages. Both stages must show good reproducibility, and a reliable method is necessary to trigger the second stage at a well-defined time during the first stage operation.

The required reproducibility of the first stage depends upon the second stage compressor coil characteristics. From experimental and theoretical investigations of the coaxial plasma accelerator with compressor coil,[8-10] the following averaged values were obtained. Time during which the pressure and the density are high enough to provide acceleration: 15 μsec. Position from the end of the light gas gun barrel along the axis of the compressor coil at which acceleration occurs: 8.5 ± 1.5 cm. With 4 km/sec final velocity of the first stage, the position accuracy becomes: ± 6 μsec. Reproducibility of the second stage: ± 3 μsec.

The requirement for timing derived from the position in the compressor coil is the most restrictive one. The light gas gun first stage must show a reproducibility of $\pm$ 3 μsec because the reproducibility of the second stage must be taken into account. A specific loading process of the light gas gun was developed to obtain the required reproducibility. The projectiles used were 595- to 600-micron diameter glass beads with a density of 2.5 g/cm^3 and a mass of 2.74×10^{-4}g. The beads were inserted into the light gas gun barrel between layers of aluminum oxide powder to provide good spread and minimum clumping.

Special effort was made to insure that each loading was as identical as possible. In addition to the standard procedures used to clean and set up the powder charge, the pump tube and the high-pressure section, the barrel and the barrel holder were checked carefully. The barrel had to be replaced frequently because it showed damage from the current discharge. Calibration tests of the first stage light gas gun were performed to determine the time after the muzzle flash at which the beads leave the barrel and their velocity. The time was determined with high-speed image converter cameras located in front of two windows in the test range. A transient light detector was focussed through one window on the end of the barrel. The muzzle flash triggered the light detector, which, in turn, triggered a delay generator. After a preset delay, an image converter camera is fired and a shadowgraph is taken of the beads emerging from the barrel. These experiments showed that the beads emerged from the barrel at 80.0 $\pm$ 2.0 μsec after the muzzle flash.

The velocity was measured with three photomultiplier tubes mounted along the test range. This standard procedure showed that the beads have an average velocity of 3.8 $\pm$ 0.2 km/sec. These values and their reproducibility are within the limits derived from the second stage characteristics.

Before the two-stage experiments were started, a theoretical analysis was made to obtain values for the setting of the delay generator. This delay setting is used to adjust the timing of the first and the second stage.

III. Theory of the Two-Stage Acceleration

The performance of the light gas gun first stage was not changed. The velocity of the beads and the time when the beads left the light gas gun barrel were kept within the limits described in the preceding section. Therefore, no theoretical analysis of the acceleration of the projectiles in the light gas gun is necessary, and the experimental values for position and velocity of the beads leaving the first stage become the initial values for the calculation of the acceleration in the second stage.

The theoretical investigation begins with the theory for the equivalent circuit for the capacitor bank with coaxial accelerator and compressor coil. Then the electromagnetic field inside the compressor coil and the plasma flow are calculated. Finally, a theory for the acceleration of the projectiles by aerodynamic drag forces is used to determine the influence of the timing of the two stages on the final velocity of the projectiles.

A. Equivalent Circuit

The capacitor bank discharge can be simulated by the two mesh transient circuits shown in Fig. 5. The coaxial accelerator is represented by the variable inductance L_2 and the compressor coil by the variable inductance L_1. The switch in the right-hand mesh simulates the beginning of the discharge between the center electrode of the coaxial accelerator and the compressor coil which occurs as the plasma moves into the compressor coil. The resistance between the center electrode and the compressor coil decreases as the plasma moves through the compressor coil; this is simulated by a variable resistance R_1. This equivalent circuit is described by two equations:

$$U_0 - \frac{1}{C_0}\int_0^t (I_1+I_2)\,\mathrm{d}t = L_0 \frac{\mathrm{d}}{\mathrm{d}t}(I_1+I_2) + R_2(I_1+I_2) + R_1 I_2 + \frac{\mathrm{d}}{\mathrm{d}t}(L_1 I_1) \tag{1}$$

$$U_0 - \frac{1}{C_0}\int_0^t (I_1+I_2)\,\mathrm{d}t = L_0 \frac{\mathrm{d}}{\mathrm{d}t}(I_1+I_2) + R_2(I_1+I_2) + \frac{\mathrm{d}}{\mathrm{d}t}(L_2 I_2) \tag{2}$$

The variations of L_1 and R_1 are approximated by linear functions of time, the gradients of these functions are used to adjust the theory to the experiment.[8] The variation of L_2 is determined from the acceleration of the plasma in the coaxial accelerator:[9]

$$\mathrm{d}^2z/\mathrm{d}t^2 = bI_1^2/2m; \qquad b = \mu \ln a/2\pi \tag{3}$$

$$L_2 = L_{20} + bz; \qquad L_{20} = L_2 \text{ at } t=0 \tag{4}$$

The compressor coil current and the capacitor bank voltage have been calculated and compared with the experimental results for the one-stage version of the coaxial accelerator with compressor coil in Ref. 8. These curves are also shown in

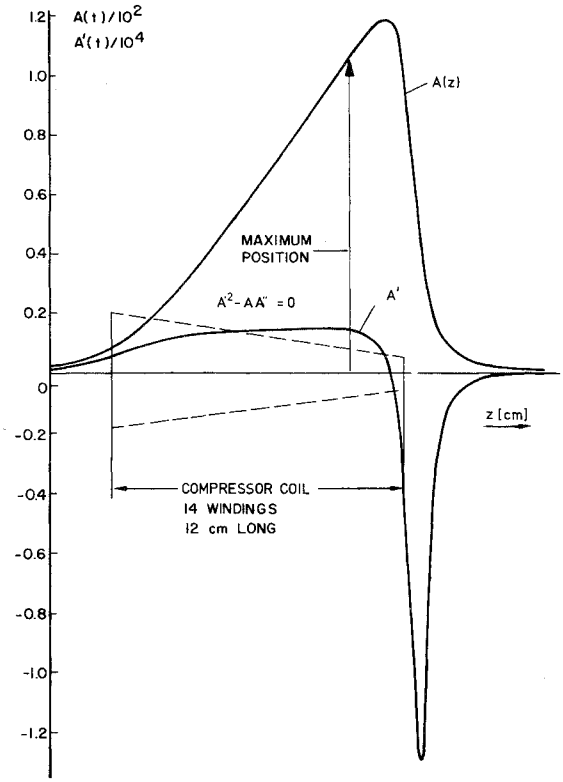

Fig. 6 Magnetic field function $A(z)$ and $dA(z)$ for conical coil with linear current distribution.

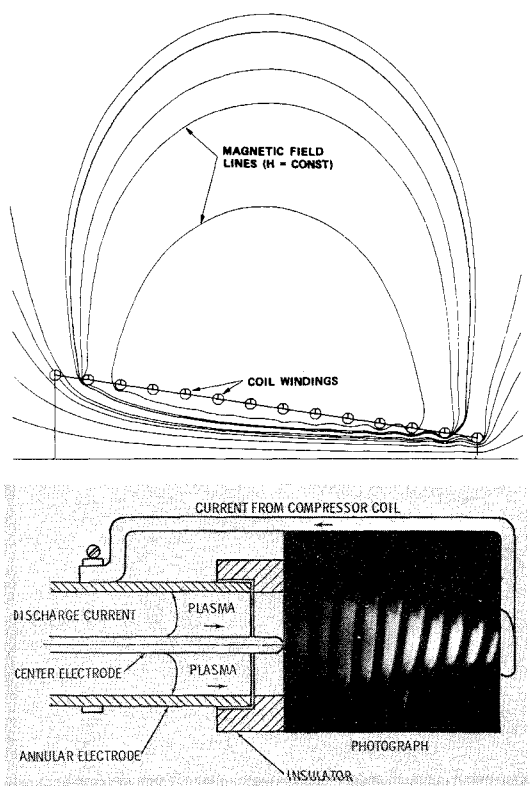

Fig. 7 Magnetic field lines and photograph of plasma flow.

Fig. 5. Photographs of the beads accelerated by the plasma flow from a Mylar foil which was placed across the end of the compressor coil before the discharge show that the acceleration occurs approximately when the compressor coil current is at its first maximum. The experimental and theoretical curves for I_l in Fig. 5 agree satisfactorily until the first maximum is reached; the theoretical results from the equivalent circuit may, therefore, be used for further calculations.

B. The Electromagnetic Field and the Current Density

For calculation of the magnetic field in the compressor coil, it was assumed that the current from the center electrode to the compressor coil creates a constant current density to the coil which leads to a linear increase of the electrical current in the windings of the coil. The coil is insulated at the wide end which is mounted on the end of the coaxial accelerator. The current increases, therefore, from zero at this end to its maximum value at the narrow (downstream) end. A parabolic current distribution was found through a theoretical investigation of an equivalent circuit with as many meshes as windings[10] to change the position of optimum acceleration of the projectiles in the compressor coil 6 mm downstream in the coil configuration used here. The magnetic field on the coil axis is

$$H_z(z,t) = I_l(t)A(z) \tag{5}$$

$A(z)$ is a function of the compressor coil geometry only. Cylindrical coordinates are used throughout the analysis, and the magnetic induction is $\bar{B} = \mu\bar{H}$. The axial magnetic field in the vicinity of the coil axis can be set approximately equal to the value on the axis. The radial magnetic field $H_r(r, z, t)$ in the vicinity of the axis is then calculated from the condition div $\bar{H} = 0$ in which the azimuthal field was assumed to be zero because of the cylindrical symmetry. This is only correct for the contribution of the compressor coil, whereas the azimuthal field of the axial current in the plasma is described in Eq. (10).

$$H_r(r,z,t) = -\frac{r}{2} I_l(t) \frac{dA(z)}{dz} \tag{6}$$

The azimuthal component of the magnetic field is produced by the axial current from the center electrode to the compressor coil. The functions $A(z)$ and $[dA(z)/dz]$ are plotted in Fig. 6. The magnetic field lines computed with an exact theory[10] are shown together with a photograph of the plasma flow in Fig. 7. The electrical field is given by

$$\bar{E} = \bar{E}^* + \bar{v} \times \bar{B} \tag{7}$$

where $\bar{E}^*$ is the sum of the electrical field between the center electrode and the compressor coil and the electrical field induced by the variation of the magnetic field with time. The term $\bar{v} \times \bar{B}$ describes the interaction between the plasma flow and the magnetic field. With the Ohm's law $\bar{j} = \sigma\bar{E}$, the current density in the compressor coil can be calculated.

For the calculation of the compression of the plasma flow toward the compressor coil axis the azimuthal and the axial components of the current density are required. The azimuthal electrical field $\bar{E}^*$ is obtained from the differentiation of the axial magnetic field from Eq. (5) with respect to the time and integration of the partial differential equation, which is given by the azimuthal component of the induction equation $\nabla \times \bar{E}^* = -\mu\dot{\bar{H}}$. The azimuthal component of the second term of Eq. (7) is reduced to the contribution of the interaction of the axial velocity with the radial magnetic field because the radial velocity is at least one order of magnitude smaller than the axial velocity. The azimuthal current density is then

$$j_\phi = -\sigma\mu r(A\dot{I} + v_z \cdot A'I)/2 \tag{8}$$

The axial current density is obtained with the assumption that the axial current from the coaxial accelerator center electrode

to the compressor coil is confined to an axial column which has the radius of the coaxial accelerator center electrode R_e. The current density in this column must show a linear decrease along the axial coordinate z from the maximum value at $z=0$ to zero at $z=L$, where L is the compressor coil length, to provide the constant radial current density which is necessary to obtain a linear increase of the current in the compressor coil for the magnetic field calculation in Eq. (5). The axial current density is

$$j_z = I\ (1-z/L)/2\pi R_e^2 \tag{9}$$

The azimuthal magnetic field inside this column is

$$H_\phi = (I_r/2\pi R_e^2)\ (1-z/L) \tag{10}$$

with $r \leq R_c$.

C. Theory of Plasma Flow

The plasma flow is described by the nonviscous magnetogas-dynamic momentum equation

$$\rho \mathrm{d}\bar{v}/\mathrm{d}t = -\nabla p + \bar{j}\times\bar{B} \tag{11}$$

$$\rho\left[\frac{\partial v_r}{\partial r} + v_r\frac{\partial v_r}{\partial r} + \frac{v_\phi}{r}\frac{\partial v_r}{\partial \phi} + v_z\frac{\partial v_r}{\partial z} - \frac{v_\phi^2}{r}\right] = -\frac{\partial p}{\partial r} + j_\phi B_z - j_z B_\phi \tag{12}$$

An estimate of the order of magnitude of the terms on the left-hand side of Eq. (12) can be made using the characteristic dimensions of the compressor coil. The coil length is L, the difference between the maximum and the minimum coil radius R, and the time required by a plasma element to flow axially through the coil is T. Then the axial velocity of the plasma is of the order of L/T and the radial velocity is of the order of R/T. This shows that the radial velocity is of one order of magnitude smaller than the axial velocity because $L \simeq 10R$. If the velocities and their derivatives in the terms on the left-hand side of Eq. (12) are replaced by these estimates for the order of magnitude and if the cylindrical symmetry is accounted for, then the left-hand side of Eq. (12) can be set equal to zero if the variation of the radial velocity with time is neglected. This can only be done to approximate a period of time which is short compared with the period of the compressor coil current. The acceleration time of the projectiles is less than 5 μsec, and the period of the compressor coil current is around 100 μsec. The time-dependent term in Eq. (12) can, therefore, be neglected for the calculation of the acceleration of projectiles.

Equation (11) is then a first-order differential equation for the pressure $p(r, z, t)$, which can be integrated radially from the compressor coil radius to the axis using Eqs. (6) and (9) for the magnetic field and (7) and (8) for the current density. This gives the pressure along the compressor coil axis as a function of time.

$$p(z,t) = \frac{\sigma\mu^2 r_c^2 AI}{2}\ (A\dot{I} + v_z A' I) + \frac{\mu I^2}{4\pi^2 R_e^2}\ (1-z/L)^2 \tag{13}$$

The second term contributes only inside the column $r=R_e$ because the axial current density is zero for $r>R_e$ and is small in the vicinity of $z=L$.

The pressure at the compressor coil $(r+r_c)$ has been set at zero because the experiments are performed in a vacuum below 20 μ. The density of the plasma flow is obtained from the equation for the polytropic change of state and the equation for an ideal gas.

$$p/\rho k = \text{const.},\quad p/\rho = R\cdot T \tag{14}$$

The density of the plasma along the axis of the compressor coil becomes a function of the local pressure from Eq. (13) and the temperature inside the coaxial accelerator which is used as the reference temperature

$$\rho = (p/p_r)\ \exp\ [(k-1)/k]\cdot(p/RT_R) \tag{15}$$

The polytropical exponent k can vary between 1.4 and 1.0. Its value does not change the shape of the density curve but only its amplitude. It will, therefore, not influence the position at which the maximum density occurs or the timing of the first and the second stage of the two-stage accelerator. The value of the polytropical exponent was set equal to one, implying that the plasma temperature does not change much between the coaxial accelerator and the compressor coil. Then the first term in Eq. (15) becomes equal to 1. For the gas constant R, a constant value was used which was taken from theoretical calculations of aluminum plasma.[11]

D. Theory of the Projectile Acceleration

The projectile in the plasma flow experiences a gasdynamic drag force which is described by

$$\bar{F} = [c_D\cdot\frac{\rho}{2}\ (v_z - v_p)^2 + \nabla p\cdot\Delta z]S \tag{16}$$

The drag coefficient c_D is set constant and equal to 1 using the Newtonian approximation for hypersonic flows. The second term of the equation describes the force resulting from a pressure gradient in the flow where Δz is a characteristic length of the projectile. Both terms are multiplied with the projectile cross section S. The density in the dynamic term is calculated according to Eq. (15) from Eq. (13) in which the second term has not been taken into account because numerical calculation showed that this term does not contribute significantly to the acceleration of the projectile. The axial derivative of this equation for the pressure $p(z,t)$ determines the density and the pressure gradient.

The same estimate of the order of magnitude is applied to the left side of the terms of the axial component of the momentum Eq. (11) which has been described for the radial term. The result is similar and shows that the change of the axial plasma velocity v_z is small if the partial derivative with respect to the time is neglected.[12] Then a first approximation will give a constant axial velocity v_z. The constant value of v_z is set equal to the velocity of the plasma when it leaves the coaxial accelerator. The theoretical value of v_z is obtained from the integration of the Eq. (3). It has been compared with experimental results in Ref. 8.

The equation of motion for the projectile is

$$\mathrm{d}v/\mathrm{d}t = [(c_D/2)\ [p(z,t)/RT_R]\ (v_z - v_p)^2 + [\mathrm{d}p(z,t)/\mathrm{d}z]\ \Delta z]\cdot(S/m_p) \tag{17}$$

where m_p is the mass of the projectile. With $\partial v_z/\partial z = 0$ because $v_z = \text{const}$

$$\frac{\mathrm{d}v}{\mathrm{d}t} = [\ c_D\ \frac{\sigma\mu^2 r_c^2 AI}{4RT_R}\ (A\dot{I} + v_z A' I)(v_z - v_p)^2 + \frac{\sigma\mu^2 r_c^2 \Delta z}{2}\ [2AA'I\dot{I} + v_z I^2(A'^2 + AA'')\ ]\ \frac{S}{m_p} \tag{18}$$

I is only a function of time, and the second term of Eq. (13) is neglected. This equation can be integrated numerically; the initial values are the position and the velocity of the projectiles, which are determined from the comparison with the experiment.

An analysis of the order of magnitude of the terms of Eq. (18) shows that the acceleration by the pressure gradient is much smaller than the dynamic term and that the azimuth current density arises mainly from the interaction between the radial magnetic field and the axial plasma flow. Then only one term remains on the left-hand side for a first approximation:

$$dv/dt = c_D(r_c^2\mu^2\sigma)/4RT_R\, I^2 v_z AA'(v_z - v_p)^2(A_p/m_p) \tag{19}$$

The position and the time of maximum acceleration of the projectiles can be calculated from the partial derivatives of Eq. (19) with respect to the axial coordinate and the time. These are then set equal to zero, and the optima are determined. The position for maximum acceleration can be calculated from the derivative with respect to z:

$$A'^2 + AA'' = 0 \tag{20}$$

The position is a function of the axial coordinate z only. It can be calculated for a specific compressor coil configuration and current density distribution. The values are indicated in Fig. 6 for a compressor coil with 2-cm initial radius, 0.5 cm end radius, and linear current density distribution.

The time for maximum acceleration can be determined with the results of the integration of the differential equations for the equivalent circuit or the experimental results shown in Fig. 5. From the differentiation of Eq. (19) with respect to the time, the condition

$$\dot{I} = 0 \tag{21}$$

for the maximum is obtained which corresponds to the first maximum of the compressor coil current.

This analysis shows that for maximum acceleration the projectile should be about 9 cm inside a 12-cm-long compressor coil at the time of the first compressor coil maximum. This is not necessarily the optimum timing for the two stages of the accelerator, but it will probably be close to it and was used for the timing of the first two-stage experiments. After these experiments had shown the feasibility of the two-stage acceleration, the set of Eqs. (1-3) and (18) was integrated numerically using a standard routine.

IV. Theoretical and Experimental Results

In the experiment the timing between the first and the second stage is adjusted through the delay setting between the light gas gun muzzle flash and the trigger pulse to the thyratron firing circuit of the second stage. For the theoretical investigation, this delay is converted into the position of the projectile at the time when the integration of the equations describing the discharge of the capacitor bank is started.

$$z = [t - 80.0)v_0 \tag{22}$$

The coordinate $z_0 = 0$ is at the wide end of the compressor coil which is mounted at the coaxial accelerator end. In the configuration used in the experiments described here $z_0 = 0$ coincides with the end of the light gas gun barrel. A variation of the delay t_d is then equivalent to a variation of the initial position.

Figure 8 shows the theoretical two-stage velocity as a function of the delay setting for various values of the capacitor bank charging voltage. The delay for maximum velocity decreases with higher charging voltage because the plasma velocity increases. The projectile velocity, together with the time of the end of the acceleration and the compressor coil

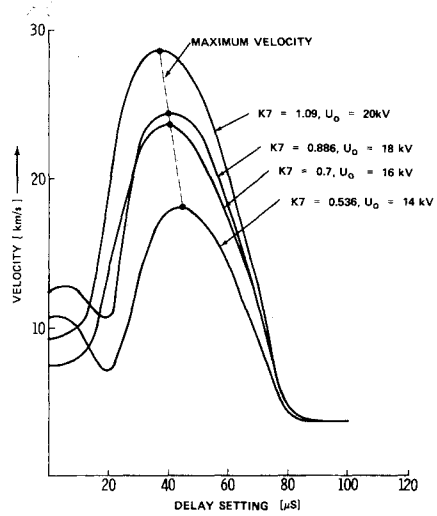

Fig. 8 Theoretical velocity as function of delay setting for 14, 16, 18, and 20 kv capacitor bank charging voltage.

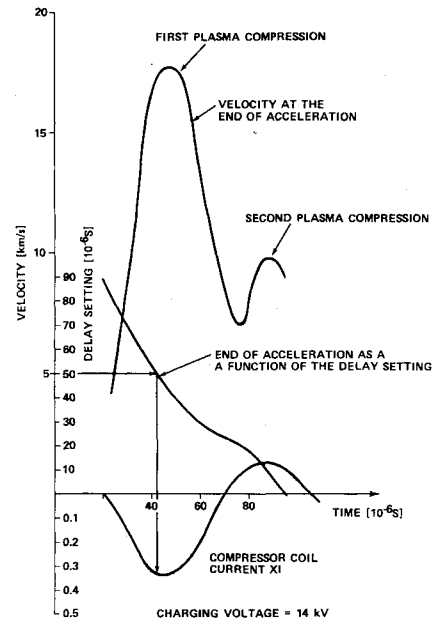

Fig. 9 Theoretical curves for velocity, end of acceleration, and compressor coil current.

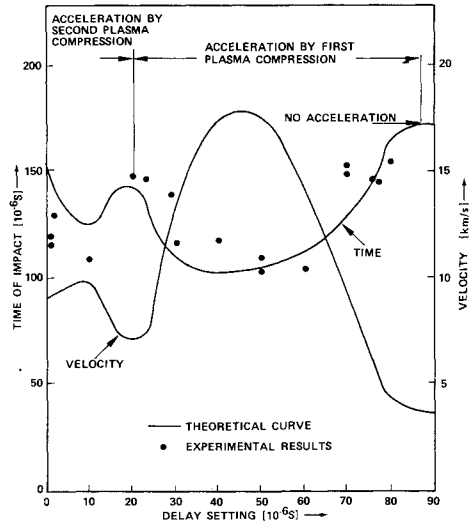

Fig. 10 Theoretical and experimental curves for time interval at 14 kv together with the theoretical velocity as a function of the delay setting.

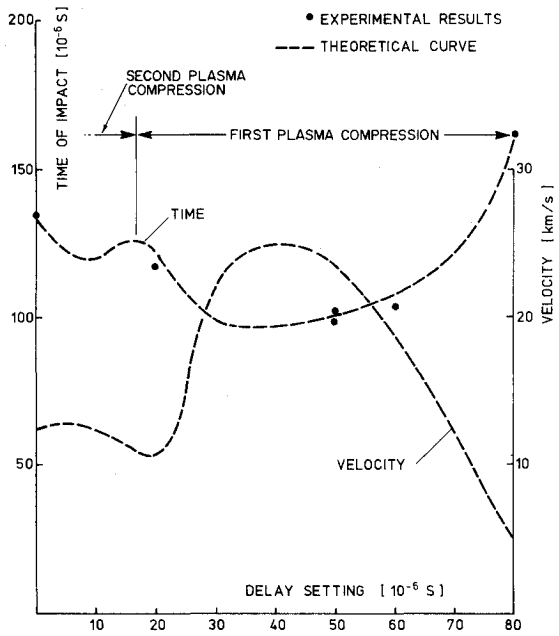

Fig. 11 Theoretical and experimental curves for time interval at 18 kv together with the theoretical velocity as a function of the delay setting.

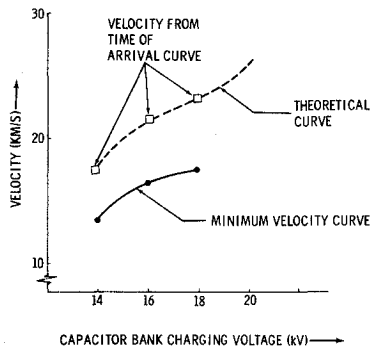

Fig. 12 Projectile velocity as a function of capacitor bank voltage for optimum final velocity delay setting.

current, is shown in Fig. 9. The maximum velocity is obtained when the acceleration ends, approximately at the time of the first compressor coil maximum. The curves in Fig. 9 are from the same calculations which were made for the timing of the two-stage experiments. A variation of the delay setting equivalent to the inaccuracy of the operation of the first and the second stages leads to large changes in projectile velocity. From the curves shown in Fig. 9, up to 4 km/sec velocity change is obtained for a 5-μsec time change. This example shows the importance of the timing of the two stages.

In the experiments the time interval between the light flash at the muzzle of the light gas gun barrel and the impact of the beads at the impact detector was recorded (see Fig. 4). This time interval has the maximum value for minimum projectile velocity, i.e., if only the light gas gun is used. When the plasma gun is added, the time interval decreases and reaches the minimum value for optimum timing or maximum final velocity.

Figure 10 shows the theoretical curve and the experimental results. The good agreement of both the theoretical and experimental curves indicates that the theoretical model provides adequate timing for the two-stage accelerator. In the same figure, the theoretical velocity is plotted; the maximum theoretical value is 17.9 km/sec. Because no other projectile velocity measurement was made, the actual velocity of the projectile is not known. It must, however, be between the maximum theoretical value and a hypothetical minimum velocity of 14.0 km/sec, which is computed from the distance between the light gas gun barrel end and the recorded time interval minus the calibrated delay of 80 μsec. This minimum velocity implies that the projectile is accelerated to its final velocity without delay as it leaves the light gas gun barrel. It can be assumed that the actual velocity is closer to the theoretical velocity because the experimental and theoretical curves for the time interval between muzzle flash and impact agree well. The curves for the theoretical velocity in Figs. 8-10 and the curves for the time interval in Fig. 10 show a second acceleration. Figure 9 shows that this second acceleration occurs at the time of the second maximum of the compressor coil current. This indicates that there are several subsequent plasma accelerations and compression phases, as predicted in Ref. 8.

Figure 11 shows theoretical and experimental results when the charging voltage was increased from 14 kV to 18 kV. The projectile velocity is shown as a function of the charging voltage in Fig. 12. The charging voltage was limited by the rating of the capacitor bank and the ignitrons. From the results obtained, it can be assumed that glass beads with a diameter of 600 μ have been accelerated to a velocity near 20 km/sec.

V. Conclusions

The diameter of glass beads that can be accelerated to 20 km/sec (250 μ in the single stage plasma accelerator,[13] has been increased by a factor of 2.4. The experiments carried out thus far exceed the performance of all other devices used for micrometeoroid simulation (see Fig. 1). These results were obtained with a first and a second stage, which had been used as single-stage accelerators previously. No other attempt was made to optimize the two-stage accelerator described here except the timing of the two stages. It may, therefore, be expected that further theoretical and experimental work will lead to another increase in the mass and the velocity of the accelerated projectiles.

References

[1] Ruppe, H.O., *Introduction to Astronautics,* Vol. 2, Academic Press, New York-London, 1967.

[2] Weidner, D.K., ed., "Space Environment Criteria Guidelines for Use in Space Vehicle Development (1969 Revision)," 2nd ed., TM X-53957, 1970, NASA.

[3] Clifton, S., "Television Studies of Faint Meteors," *Journal of Geophysical Research,* Vol. 78, Oct. 1973, pp. 6511-6521.

[4] Cable, A.J., *High Velocity Impact Phenomena,* edited by R. Kinslow, Academis Press, New York-London, 1970.

[5] Moore, E.T., "Explosive Gas Gun for Hypervelocity Acceleration," presented at the 4th Symposium on Hypervelocity Technology, North American, Rockwell, Tullahoma, Tenn., 1965.

[6] Scully, C.N. and Cowan, P.L., "Hypervelocity Gun for Micrometeorite Impact Simulation Employing Capacitor Discharge in a Condensed Phase," presented at the 4th Symposium on Hypervelocity Impact, North American, Rockwell, Tampa, Fla., 1960.

[7] Becker, D.G., "A Linear Accelerator for Simulated Micrometeors," *Review of Scientific Instruments,* Vol. 44, June 1973, p. 755.

[8] Igenbergs, E. and Shriver, E., "Magnetogasdynamic Compression of a Coaxial Plasma Accelerator Flow for Micrometeoroid Simulation," *Journal of Applied Physics,* Vol. 44, June 1973, pp. 2177-2187.

[9] Shriver, E.L., "Analytical and Experimental Investigation of the Coaxial Plasma Gun for Use as a Particle Accelerator," TN D-6687, April 1972, NASA.

[10] Kuczera, H., "Zur Berechnung des stationären Magnetfeldes von Spulen und der Ermittlung des Feldlinienverlaufs," Bericht 73-4 des Instituts für Raumfahrttechnik der Technischen Universität München; Munich.

[11] Todd, F., "The Transient Properties of Dense Plasmas," NASA Contract Rept. NAS 8-25055, April 1971.

[12] Igenbergs, E., "Magnetogasdynamische Kompression eines Plasmas zur Beschleunigung von Teilchen für die Simulation von Mikrometeorioden," Deutsche Luft-, and Raumfahrt, Mitteilung 73-15, May 1973.

[13] Igenbergs, E.B., "Ein magnetogasdynamischer Beschleuniger für die Simulation von Mikrometeoriden," *Raumfahrtforschung,* Heft 4, Juli/Aug. 1973.